Journal of Magnetic Resonance 234 (2013) 112–124

Contents lists available at SciVerse ScienceDirect

Journal of Magnetic Resonance

journal homepage: www.elsevier.com/locate/jmr

Spectrally edited 2D ^{13}C—^{13}C NMR spectra without diagonal ridge for characterizing ^{13}C-enriched low-temperature carbon materials

Robert L. Johnson [a,c], Jason M. Anderson [b,c], Brent H. Shanks [b,c], Xiaowen Fang [a], Mei Hong [a], Klaus Schmidt-Rohr [a,c,*]

[a] Department of Chemistry, Iowa State University, Ames, IA 50011, United States
[b] Department of Chemical and Biological Engineering, Iowa State University, Ames, IA 50011, United States
[c] Center for Biorenewable Chemicals (CBiRC), Iowa State University, Ames, IA 50011, United States

ARTICLE INFO

Article history:
Received 25 March 2013
Revised 4 June 2013
Available online 22 June 2013

Keywords:
Spectral editing
Black carbon structure
Char structure
Melanoidin structure
Furan rings
Ketones
Double-quantum NMR

ABSTRACT

Two robust combinations of spectral editing techniques with 2D ^{13}C—^{13}C NMR have been developed for characterizing the aromatic components of ^{13}C-enriched low-temperature carbon materials. One method (exchange with protonated and nonprotonated spectral editing, EXPANSE) selects cross peaks of protonated and nearby nonprotonated carbons, while the other technique, dipolar-dephased double-quantum/single-quantum (DQ/SQ) NMR, selects signals of bonded nonprotonated carbons. Both spectra are free of a diagonal ridge, which has many advantages: Cross peaks on the diagonal or of small intensity can be detected, and residual spinning sidebands or truncation artifacts associated with the diagonal ridge are avoided. In the DQ/SQ experiment, dipolar dephasing of the double-quantum coherence removes protonated-carbon signals; this approach also eliminates the need for high-power proton decoupling. The initial magnetization is generated with minimal fluctuation by combining direct polarization, cross polarization, and equilibration by ^{13}C spin diffusion. The dipolar dephased DQ/SQ spectrum shows signals from all linkages between aromatic rings, including a distinctive peak from polycondensed aromatics. In EXPANSE NMR, signals of protonated carbons are selected in the first spectral dimension by short cross polarization combined with dipolar dephasing difference. This removes ambiguities of peak assignment to overlapping signals of nonprotonated and protonated aromatic carbons, e.g. near 125 ppm. Spin diffusion is enhanced by dipolar-assisted rotational resonance. Before detection, C—H dipolar dephasing by gated decoupling is applied, which selects signals of nonprotonated carbons. Thus, only cross peaks due to magnetization originating from protonated C and ending on nearby nonprotonated C are retained. Combined with the chemical shifts deduced from the cross-peak position, this double spectral editing defines the bonding environment of aromatic, COO, and C=O carbons, which is particularly useful for identifying furan and arene rings. The C=O carbons, whose chemical shifts vary strongly (between 212 and 165 ppm) and systematically depend on their two bonding partners, show particularly informative cross peaks, given that one bonding partner is defined by the other frequency coordinate of the cross peak. The new techniques and the information content of the resulting spectra are validated on sulfuric-acid treated low-temperature carbon materials and on products of the Maillard reaction. The crucial need for spectral editing for correct peak assignment is demonstrated in an example.

1. Introduction

Carbon materials produced from renewable feedstocks at moderate temperatures, including hydrothermal carbon [1] and chars [2], are attractive for a variety of applications, including as catalyst supports [3,4], lithium-ion battery anodes [3,5], absorbents to remove environmental contaminants such as metals [6], and for soil amendments and carbon sequestration [7,8]. Carbon-rich materials produced by fires or pyrolysis, including oxidized char residues in soil [9], are generally of interest in environmental science [10,11]. Other chemical transformations producing aromatic compounds at moderate temperatures are sugar caramelization [12] and the Maillard reaction between reducing sugars and amine compounds [13–15], which are relevant in food science. Furthermore, oxygen-containing carbon structures are of interest in the production of graphene from graphite oxide [16,17].

Solid-state ^{13}C NMR is the best available method for characterizing the overall composition and local structure of such amorphous, carbon-rich materials that also contain oxygen in a

* Corresponding author. Address: Chemistry Dept., Hach Hall, Ames, IA 50011, United States.
E-mail address: srohr@iastate.edu (K. Schmidt-Rohr).

1090-7807/$ - see front matter © 2013 Published by Elsevier Inc.
http://dx.doi.org/10.1016/j.jmr.2013.06.006

variety of functional groups [1,8–11,13–24]. However, even by NMR the various aromatic structures are often difficult to identify. As seen in Fig. 1, the aromatic-carbon regions (100–155 ppm) of the ^{13}C NMR spectra of low-temperature carbon materials often exhibit strongly overlapping bands, which can be attributed to furans, phenols, other individual or fused six-membered arene rings, and possibly pyrroles.

The main challenge in the spectral analysis of aromatic-carbon rich materials arises from ambiguities in the assignment of a signal at a certain ppm value to a specific type of carbon. For instance, a peak near 123 ppm can be due to C—H in six-membered aromatic rings (in particular when they are fused or heavily substituted) or arise from aromatic C two bonds from O, i.e. C=C—O in furan or phenol rings. Aromatic C—O resonating at 150 ppm can be due to furan or phenol rings, which are difficult to distinguish in one-dimensional NMR because of the similar local bonding structure of their aromatic carbons (highlighted by dashed outlines in Scheme 1). Signal at 162 ppm can be from C—O in a phenol or from COO bonded to a furan ring, and bands at 180 ppm may arise from COO bonded to alkyl C, or from C=O bonded to a furan ring (see below) [25]. Furthermore, in the presence of furans and/or phenols, the signals of nonpolar arenes (120–145 ppm) are often "sandwiched" between those of aromatic C—O (140–160 ppm) and C—C—O (100–130 ppm) and therefore difficult to resolve.

Even two-dimensional ^{13}C—^{13}C NMR of ^{13}C-enriched materials, which identifies carbons in close proximity in terms of cross peaks at the carbons' frequency positions, often cannot resolve the ambiguities mentioned above. In particular, arene signals, which are observed typically near 130 ppm, are mostly overlapped by the dominant diagonal ridge in 2D exchange NMR spectra, see Fig. 2, or may remain sandwiched between furan peaks [24]. Fig. 2 also indicates that cross peaks between sp^2- and sp^3-hybridized carbons may be impacted by spinning sidebands of the diagonal ridge.

Here we show how these problems can be eliminated by two methods incorporating suitable spectral editing into ^{13}C—^{13}C correlation NMR. The first technique specifically correlates signals of protonated and nonprotonated carbons, the second method the peaks of two nonprotonated carbons. While the former can identify arenes convincingly, the latter is particularly suitable for characterizing the substituents of the various aromatic rings and the presence of clusters of fused aromatic rings. In both experiments, the positions of the observed cross peaks of ketone (C=O) carbons are very informative due to their systematic dependence on their two bonding partners. For instance, the chemical shifts for C=O with two ethyl vs. two furan substituents differ by more than 40 ppm. Different substitution patterns of furans (e.g. only on Cα, or on both Cα and Cβ, see Scheme 1a) can be identified. Both experiments remove the overwhelming diagonal ridge and its associated spectral artifacts (see Fig. 2), thus enabling detection of cross peaks near and on the diagonal, as well as improving the dynamic range, which benefits detection of cross peaks of low intensity. We demonstrate both experiments on ^{13}C-enriched glucose carbonized by fuming sulfuric acid, 350 °C glucose char treated with fuming sulfuric acid, and two melanoidins made from ^{13}C-enriched glucose

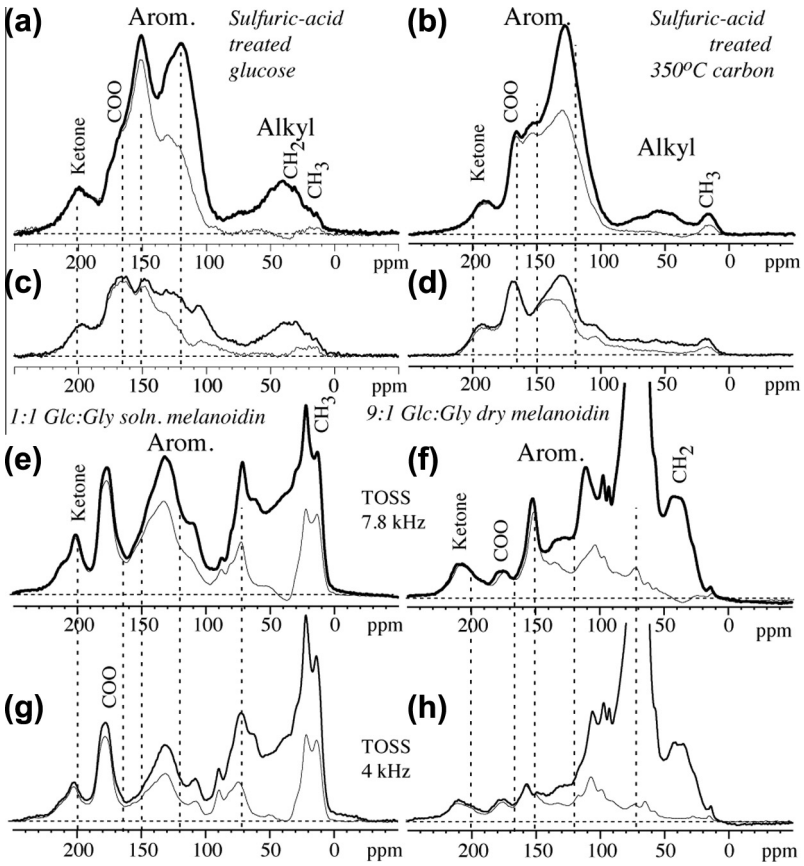

Fig. 1. ^{13}C CP/TOSS NMR spectra (thick lines) and corresponding spectra after 40 μs of dipolar dephasing (thin lines) of (a and c) glucose after treatment with fuming sulfuric acid ("DirfumS"); (b and d) glucose pyrolyzed at 350 °C and then treated with fuming sulfuric acid ("Pyr350fumS"); (e and g) 1:1 glucose:glycine melanoidin from Maillard reaction in solution ("Mel1:1"); (f and h) 9:1 glucose:glycine melanoidin from dry Maillard reaction ("Mel9:1"). All samples were made from uniformly (>99%) ^{13}C-enriched glucose. (a, b, e, and f) were obtained at 7.8 kHz MAS, (c, d, g, and h) at 4 kHz, where aromatic-carbon signals are reduced, revealing COO peaks near 165 ppm in (c and d). Vertical dashed lines at 200, 165, 150, and 120 ppm highlight the variations in ketone (C=O), COO, aromatic C—O, and aromatic CH, positions, respectively. The dashed lines at 72 ppm in (e–h) mark the OCH/NC$_q$ peak. In (f and h), the top of the high OCH peak near 70 ppm is not shown.

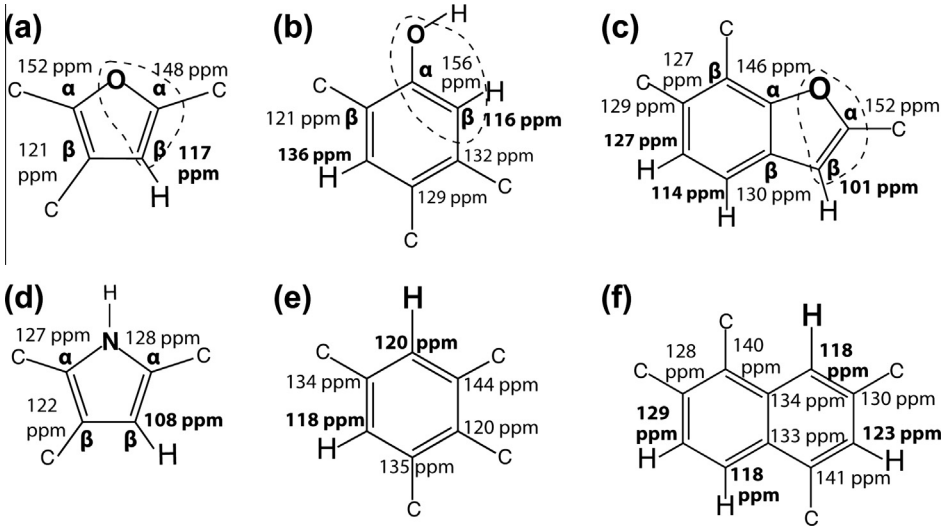

Scheme 1. Simple aromatic ring structures and typical chemical shifts, predicted by the empirical ACD/NMR program, with furan-ring, arene-ring, COO, and C=O substituents (shown here only as "C"; full structures are displayed in Scheme S1 in the Supplementary material). Substituted (a) furan; (b) phenol; (c) benzofuran; (d) pyrrole; (e) benzene; (f) naphthalene.

and glycine [13,14]. For one of the samples, we use the spectral editing to correct an erroneous structural assignment.

2. Technical aspects

2.1. Dipolar-dephased DQ/SQ NMR

Fig. 3 shows the pulse sequence for obtaining a 2D correlation spectrum with cross peaks only between signals of nonprotonated carbons, and without diagonal ridge. At the core it is a standard double-quantum (DQ)/single-quantum (SQ) pulse sequence in the tradition of the classical INADEQUATE experiment [26]. During the evolution period t_1, the two-spin double-quantum coherence evolves with the sum $(\omega_A + \omega_B)$ of the frequencies, and during detection (t_2) the magnetization precesses with the individual frequencies ω_A and ω_B. The DQ coherence is generated and reconverted by the $^{13}C—^{13}C$ dipolar couplings recoupled by a suitable rotation-synchronized pulse sequence, such as SPC5 [27], for ca. 0.3 ms; it is selected by the standard phase cycling of the second block relative to the first [26]. To keep spinning sidebands from overlapping with centerbands in the DQ dimension, the experiment needs to be applied at a sufficiently high spinning frequency. In our magnet, at 0.1 kHz/ppm, 14 kHz corresponds to 140 ppm and is just fast enough to avoid significant overlap of the sidebands and centerbands. In the SQ dimension, sidebands at $\nu_r = 14$ kHz do not interfere with the signals of interest due to their favorable location in the spectral plane.

To select the signals of nonprotonated carbons, we need to dephase the double-quantum coherences involving protonated carbons, using recoupled dipolar dephasing by gated decoupling for about 68 μs [21]. A π-pulse must be applied at the center of the delay without decoupling to recouple the C—H dipolar interaction [21] and refocus the chemical shift evolution. However, this pulse interferes severely with the DQ reconversion [27]. It could be accounted for by a fairly complicated reversal of the SPC5 DQ excitation phase sequence, as pointed out in Ref. [27]. A much simpler solution, however, is to add a compensating second π-pulse right at the end of DQ excitation, where it does not have any other significant effects.

It is important to note that dipolar dephasing *before* double-quantum excitation would not suppress the signals associated with CH carbons completely. Consider a $C_{A,nonprot}—C_BH$ pair. Magnetization of $C_{A,nonprot}$ surviving the first dipolar dephasing would evolve into a $C_{A,nonprot}—C_BH$ double-quantum coherence oscillating with $(\omega_A + \omega_B)$; after reconversion, the $C_{A,nonprot}$ signal would survive the second dipolar dephasing and be detected at ω_A. As a result, a signal at $(\omega_A + \omega_B, \omega_A)$ with the protonated-carbon frequency ω_B would survive. Thus, dephasing of the double-quantum coherence itself is needed (and the dephasing before detection is optional).

The SPC5 sequence is excellent for nonprotonated DQ NMR at 14 kHz MAS. The ^{13}C rf field of $\gamma B_1/(2\pi) = 5 \times 14$ kHz is about as strong as one can safely apply in our probe head. Being large compared to the range of chemical shifts (220 ppm or 22 kHz), it provides a broad excitation bandwidth. It also decouples the nonprotonated carbons from the protons, even without ^1H irradiation. In fact, we recorded the spectra without ^1H irradiation during SPC5, since the performance was better than with moderate-power ^1H irradiation.

The explicit selection of the signals of nonprotonated carbons removes the main technical difficulty of DQ/SQ NMR, which is the detection of the signals of aromatic CH carbons without significant attenuation. For protonated carbons, ^1H decoupling needs to be at least 2.5 times stronger than the ^{13}C irradiation during SPC5, which itself needs to be strong, about 70 kHz, for two reasons: It needs to be five times the spinning frequency of $\geqslant$14 kHz [27], and it needs to be much larger than the spread of ^{13}C frequencies (20 kHz for isotropic chemical shifts and up to 25 kHz for chemical shift anisotropy at 9.4 T). The required 2.5×70 kHz = 175 kHz ^1H radio-frequency field cannot be achieved in our 4-mm radio-frequency coil; in a smaller coil capable of generating 175 kHz without arcing, sensitivity would be seriously impaired. Detection of nonprotonated carbon signals in our edited spectra eliminates these serious difficulties and makes the experiment easy to perform.

2.2. Preparation of magnetization by combined DP and CP plus spin diffusion

At the beginning of the 2D experiment, magnetization of nonprotonated carbons must be produced efficiently and reproducibly. The standard method, cross polarization from ^1H, is not particularly efficient for nonprotonated ^{13}C at 14 kHz MAS and quite

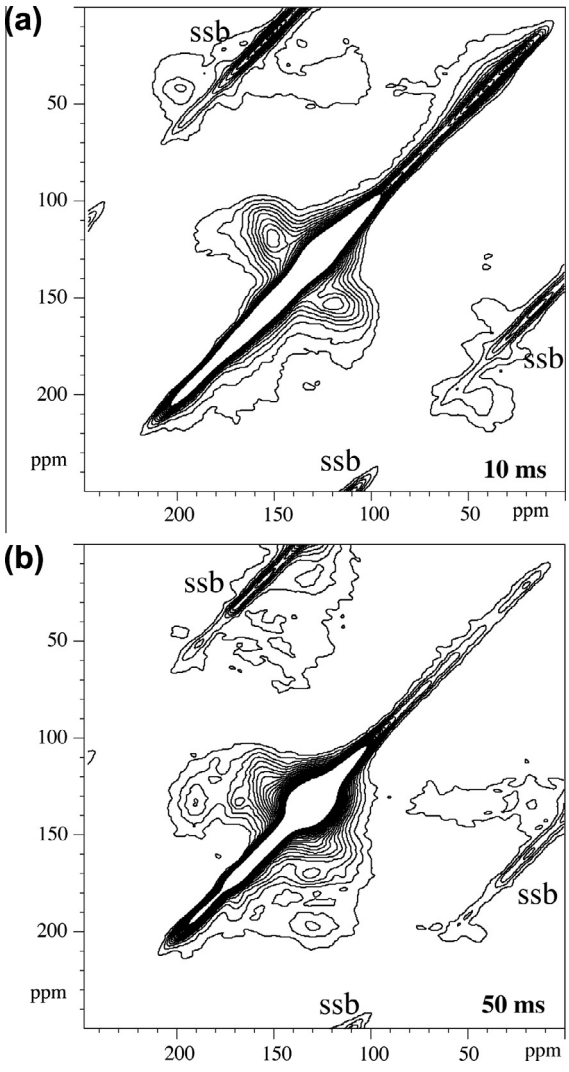

Fig. 2. Contour plots of 'regular' 2D ^{13}C—^{13}C exchange NMR spectra of (a) ^{13}C glucose charred by fuming sulfuric acid (DirfumS material), with a spin-diffusion time of t_m = 10 ms with DARR irradiation on ^{1}H, and of (b) Pyr350fumS, with t_m = 50 ms (the 10-ms spectrum was dominated by artifacts). The diagonal ridge in the aromatic region of each spectrum is above the highest contour line. "ssb": spinning sidebands of the diagonal ridge.

sensitive to fluctuations of radio-frequency power levels. We have used two simple approaches to mitigate these problems. Firstly, we combine standard 1-ms cross polarization from ^{1}H with direct polarization (DP) of ^{13}C to generate the ^{13}C magnetization at the start of the experiment [28]. The 90° pulse for direct polarization flips the ^{13}C magnetization onto the CP spin-lock field, to combine with the magnetization generated by CP [28]. Secondly, after CP a 90° pulse flips the ^{13}C magnetization to the z-direction for ~100 ms of ^{13}C spin diffusion. This transfers magnetization from the protonated to the nonprotonated C, enhancing their magnetization and minimizing intensity fluctuations due to variations in CP efficiency for the nonprotonated carbons [29–31]. The "t_1 noise" along the vertical dimension in the spectrum that such fluctuations would produce was not observed in our data, which attests to the reproducible magnetization level at the start of the 2D pulse sequence achieved by combined DP and CP plus spin diffusion.

2.3. Shearing of the DQ/SQ spectrum

We shear the dipolar dephased DQ/SQ spectrum by 45° along the ω_1 dimension in order to obtain a spectrum equivalent to a SQ–SQ exchange spectrum (but still without a diagonal ridge) [32]. This simplifies the comparison with exchange NMR spectra and provides symmetric cross peaks with respect to the diagonal, which can be a used as a criterion of spectral quality.

Specifically, the shearing displaces peaks from (ω_1,ω_2) to $(\omega_1-\omega_2,\omega_2)$. Thus, shearing of the signals of a ^{13}C spin pair with frequencies ω_A and ω_B originally at $(\omega_A+\omega_B,\omega_A)$ and $(\omega_A+\omega_B,\omega_B)$ moves them to $(\omega_A+\omega_B-\omega_A,\omega_A)$ and $(\omega_A+\omega_B-\omega_B,\omega_B)$, respectively. Thus, they appear at (ω_B,ω_A) and (ω_A,ω_B), like the cross peaks in a 2D exchange spectrum.

2.4. Exchange with protonated and nonprotonated spectral editing (EXPANSE) NMR

The second new pulse sequence, which probes the environment of protonated aromatic carbons in a simple two-dimensional experiment with favorable spectroscopic features, is shown in Fig. 4. It involves selection of only protonated-carbon signals before the evolution time, by combining short (72-μs) cross polarization with dipolar-dephasing difference (in two experiments, see below), and detection of nonprotonated carbons selected by dipolar dephasing. The complementary spectral editing removes the diagonal ridge (see below). 'Gamma averaging' [33] with the mixing time incremented in four steps of $t_r/4$ turned out to be crucial for suppressing sideband artifacts of the diagonal ridge of protonated carbons.

In our 9.4-T magnetic field, the EXPANSE experiment is applied most conveniently at ⩾14-kHz MAS. While a regular ^{13}C—^{13}C exchange NMR spectrum at 14 kHz would still contain spinning sidebands of the diagonal ridge (labeled "ssb" in Fig. 2) that overlap with real cross peaks, the removal of the diagonal ridge and its sidebands in EXPANSE NMR eliminates this problem. The evolution

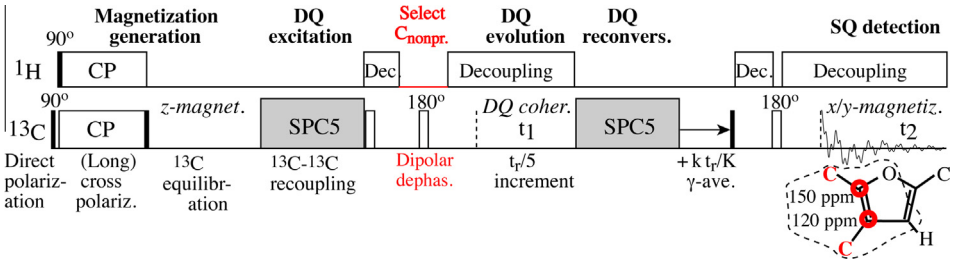

Fig. 3. Pulse sequence for 2D ^{13}C—^{13}C correlation NMR of nonprotonated carbons, without diagonal ridge, by dipolar dephased DQ/SQ NMR. Filled narrow rectangles indicate 90° pulses, twice wider open rectangles 180° pulses. Combined direct and cross polarization (CP) is followed by transfer of z-magnetization from protonated to nonprotonated C. The SPC5 homonuclear recoupling sequence [27] (shown shaded) is applied in two blocks of 4 t_r = 0.286 ms duration each to generate and reconvert double-quantum coherence. In addition to the ^{13}C 180° pulse needed for C—H dephasing of the double-quantum coherence, a second 180° pulse is applied directly after the first SPC5 block, since an odd number of 180° pulses would interfere with reconversion by SPC5. A short period after the second SPC5 block, with only z-magnetization, is incremented in K = 4 steps of $t_r/4$ to decouple the rotor phases in the evolution and detection time ("γ-averaging") and avoid dispersive spinning sidebands. The pulse program can be found at http://www.public.iastate.edu/~nmrksr/.

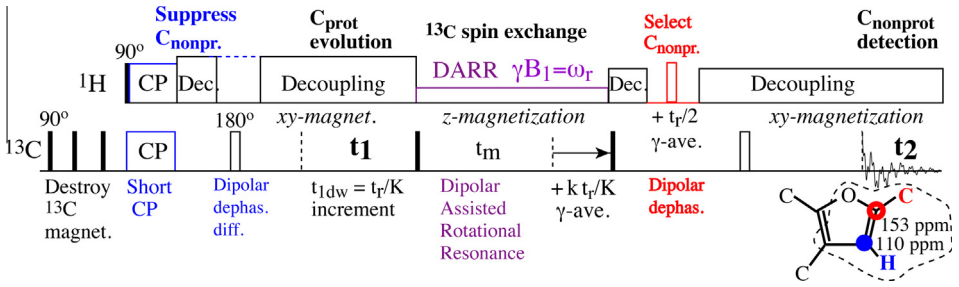

Fig. 4. Pulse sequence for spectrally edited 2D ^{13}C—^{13}C correlation by exchange with protonated and nonprotonated spectral editing (EXPANSE) NMR, without diagonal ridge. After the ^{13}C magnetization has been destroyed by a series of 90° pulses, short cross polarization of 72 μs polarizes mostly the protonated carbons. Residual signals of nonprotonated C in the ω_1 dimension are removed by dipolar dephasing difference, i.e. by running a second experiment identical to the first, except for recoupled dipolar dephasing (2 × 16 μs of gated decoupling) before the evolution time, and subtracting this signal out (scaled up by ca. 1.3 to null the residual diagonal ridge). The evolution time is incremented in two steps of $t_r/2$, and the mixing time (at a given t_1) in two steps of $t_r/2$, to suppress sideband artifacts in ω_1 by "γ-averaging". During the mixing time, ^1H irradiation at $\gamma B_1 = \omega_r$ recouples the C—H dipolar couplings and thus speeds up ^1H-driven ^{13}C spin diffusion. Before detection, signals of immobile protonated carbons are suppressed by recoupled dipolar dephasing; the position of the gated decoupling delay is shifted by $t_r/2$ during signal averaging to remove first-order chemical-shift anisotropy sideband artifacts (γ-averaging).

time is incremented in steps of $t_r/2$ or $t_r/4$, so that any higher-order spinning sideband artifacts in the ω_1 dimension coincide with the spectrum itself or with lower-order sidebands.

During the mixing time of about 10 ms, dipolar assisted rotational resonance (DARR) is applied to recouple proton-driven ^{13}C spin diffusion [34]. The spectral editing ensures that the spin exchange rate should be quite similar for all signals observed: Since only magnetization of protonated carbons is observed in the cross peaks, it is certain that a C—H coupling is present that can be recoupled by DARR and produce the zero-quantum peak overlap enabling efficient spin diffusion [35].

The pulse sequence can also be implemented at slower spinning frequencies, e.g. 8 kHz, with sideband-suppression by TOSS (total suppression of sidebands) [36] before detection and TOSS and de-TOSS (time-reversed TOSS) flanking the evolution period [37]. The dipolar dephasing can then be achieved simply by a delay of ~30 μs with decoupling gated off, without a π-pulse for recoupling. DARR should be applied even at these lower spinning frequencies, since the low proton density of many carbon materials otherwise results in undesirably frequency-selective proton-driven spin diffusion.

2.5. Selection of CH_n signals by dipolar dephasing difference

A spectrum of only protonated carbons, in particular aromatic CH, can be obtained by short cross polarization and dipolar-dephasing difference spectroscopy [38,39]. After 50 μs of CP, the signals of nonprotonated carbons will be small (~10% of their full intensity), but not negligible. They can be removed by recording and subtracting the spectrum obtained with the same parameters, except for additional dipolar dephasing after cross polarization. In this spectrum, the signals of nonprotonated C are retained at >90%, and therefore they will be reduced to <10% in the difference spectrum. The remaining intensity of the nonprotonated C is <1% (<10% of 10%), and therefore negligible.

In our 2D experiment, we implement this approach to achieve a CH_n-only spectrum in the first dimension. After short cross polarization, the dipolar dephasing difference can be obtained by recording two 2D spectra, one without the first dipolar dephasing period, the other with this dipolar dephasing, and taking their difference. To avoid artifacts from slow drifts in the experimental conditions, such as cross polarization, it is best to alternate between recording the time signal at a given value of the evolution time t_1 without and with the first dipolar dephasing period.

It should be noted that the dephasing time that produces vanishing C—H signal after short CP is significantly shorter than in "regular" experiments with direct polarization or long cross polarization. The C—H magnetization reaches zero after about 38 μs, instead of ~67 μs, without dipolar decoupling. This is primarily due to short cross polarization preferentially enhancing the magnetization of carbons with strong C—H couplings, which dephase quickly. For instance, C—H bonds along the rotor axis are always at the magic angle with the B_0 field, and therefore cross polarize slowly. They also dephase slowly, so when they are taken out of the ensemble by short CP, the total dephasing will be faster. Secondly, due to the low ^1H density in the aromatic regions, H—H dipolar couplings are too weak to dampen out the oscillation of the dephasing curve. The dephasing of the observed nonprotonated-carbon signals is also faster. At the zero crossing of the CH carbons, the nonprotonated-carbon intensity is reduced by a factor of ~1.3. This scaling factor of the dipolar dephased spectrum, applied before the subtraction from the spectrum without dephasing, is fine-tuned to remove the residual diagonal ridge completely.

In order to avoid sideband artifacts arising from spatially asymmetric modulation of the magnetization by the dipolar dephasing before detection, we applied two-step γ-averaging to it. This involved shifting the position of the gated decoupling and the 180° recoupling pulse on ^1H by $t_r/2$ in the rotation period after the mixing time and adding the resulting signals. In order to avoid timing problems, the periods before and after the 180°-pulse for the Hahn echo before detection were each extended to $\tau = 2t_r$.

2.6. Identification of the specific bonding environment

In EXPANSE NMR, the CH and $C_{nonprot}$ spectral editing, combined with chemical-shift information in the two spectral dimensions, identifies the immediate bonding environment of the two coupled aromatic carbons unambiguously: One carbon, whose signal is shown in ω_1, is bonded to hydrogen and two aromatic carbons if it resonates below 137 ppm; if the ppm value is higher, the carbon must have bonds to H, O, and aromatic C. The other carbon, detected in ω_2, is not protonated and thus bonded to three carbons, or to two C and one O, if it resonates below or above 137 ppm, respectively.

Similarly, in the dipolar dephased DQ/SQ spectrum, a chemical shift above 142 ppm can be assigned to nonprotonated C—O, below 130 ppm to nonprotonated C—C—O (two bonds from O), and signals between 127 and 142 ppm signal to nonprotonated arene C. Thus, the first and most of the second shell of bonded carbons around the carbons observed can be uniquely identified in these spectrally edited 2D experiments.

Generally, any connection between aromatic rings gives a pair of signals in the dipolar-dephased DQ/SQ, since the two linked aromatic carbons cannot be protonated (the other two of their

three bonding partners must be in their respective aromatic ring). This includes the signals of bridgehead carbons of fused aromatic rings, which will be prominent on the diagonal near 130 ppm.

2.7. Absence of the diagonal ridge

Both 2D techniques presented here provide spectra without the diagonal ridge typically observed in 2D exchange NMR. In DQ/SQ NMR, a diagonal ridge is always absent [26]. In EXPANSE NMR, the mutually exclusive spectral editing before evolution and before detection eliminates the diagonal ridge for aromatic carbons, since diagonal signals of protonated carbons are suppressed before detection and those of nonprotonated carbons before evolution; only magnetization that starts out on a protonated carbon and ends up on a nonprotonated one survives the double spectral editing. The diagonal ridge "survives", with greatly reduced intensity, only for CH_3 groups, which combine features of CH groups (they contain protonated C) with those of nonprotonated carbons (their signal is not fully eliminated by dipolar dephasing, due to partial motional averaging of the C—H dipolar couplings by the rotational jumps around the C_3 axis).

The suppression of the diagonal ridge has various advantages. For instance, the associated sideband and cut-off artifacts are eliminated and as a result, the EXPANSE experiment can be performed with short spin-exchange time, to obtain cross peaks mostly for directly bonded carbons (one-bond couplings). Removal of the diagonal ridge also permits a reduction of the number of t_1 slices needed, with a resulting reduction in the measuring time required. Even more importantly, cross peaks near or even on the diagonal (from nonprotonated C resonating at the same frequency as the CH to which it is bonded) can be observed without overlap from the diagonal ridge.

2.8. Comparison of EXPANSE with DQ/SQ NMR

The absence of a trivial diagonal ridge is a favorable feature that EXPANSE shares with DQ/SQ NMR. Otherwise, the signals observed in the EXPANSE spectrum and in the dipolar-dephased DQ/SQ spectrum are fully complementary (except those involving CH_3 groups): In EXPANSE NMR, only CH_n-group signals are observed in ω_1, while all CH- and CH_2-signals are suppressed in dipolar-dephased DQ/SQ NMR.

While the DQ/SQ experiment can probe structure only on the scale of one or two bonds, proximities on the 1-nm scale can detected in EXPANSE NMR simply by extending the mixing time in the experiment. Furthermore, the EXPANSE spectrum can provide information that is not accessible by double-quantum NMR. Consider, for instance, two protonated–nonprotonated carbon pairs resonating at (ω_A and ω_B) and (ω_B and ω_A), i.e. with complete overlap of the signals, which makes it challenging to separate them. In the dipolar dephased DQ/SQ NMR spectrum, no signal would be observed for either pair, while in a double-quantum experiment with dipolar dephasing only before detection, this combination gives the same pair of signals at ($\omega_A + \omega_B, \omega_A$) and ($\omega_A + \omega_B, \omega_B$). In the EXPANSE spectrum, cross peaks at (ω_B, ω_A) and (ω_A, ω_B) identify the two pairs of carbons uniquely.

3. Results

3.1. Sulfuric-acid carbonized glucose

Figs. 5 and 6 show spectrally edited 2D ^{13}C—^{13}C correlation spectra of two carbon materials produced by sulfuric-acid treatment, of ^{13}C-enriched glucose and of char produced from ^{13}C-glucose by pyrolysis at 350 °C; the materials are termed DirfumS and Pyr350fumS, respectively. The spectral patterns show some similarities, in particular pronounced Cβ—Cα—O cross peaks at (120 ppm, 150 ppm) with both types of spectral editing. These signals in the EXPANSE spectra must be assigned to HCβ—$C\alpha_{nonp}$—O of furan or phenol, while those in the dipolar-dephased DQ/SQ spectra are from $C\beta_{nonp}$—$C\alpha_{nonp}$—O. Signals of O—$C\alpha_{nonp}$—$C\alpha_{nonp}$—O linkages around (148 ppm, 148 ppm) are less pronounced. This may be due to the fact that $C\beta_{nonp}$—$C\alpha_{nonp}$—O can occur both intra- and intermolecularly, while O—$C\alpha_{nonp}$—$C\alpha_{nonp}$—O can occur only between furan rings. A short, broad ridge in the EXPANSE spectrum ending at (109 ppm, 120 ppm) in Fig. 5 can be assigned to furan HCβ—$C\beta_{nonp}$.

The EXPANSE spectra in Figs. 5 and 6 display a distinct ridge near (115 ppm, 180 ppm), which is assigned to two-bond HCβ—C—C=O correlations, i.e. ketones linked to the furan rings. A corresponding signal is also detected in the dipolar-dephased DQ/SQ spectrum, as is signal of furan-linked COO at ~162 ppm producing a pronounced shoulder around (125 ppm, 162 ppm) in the dipolar-dephased DQ/SQ spectrum. The COO peaks can also be verified in the one-dimensional slow-MAS TOSS spectra of Fig. 1, where the otherwise dominant aromatic signals have been greatly reduced. For the DirfumS sample, the EXPANSE spectrum also shows characteristic intensity near (150 ppm, 125 ppm). This intensity can be assigned with certainty to furan O—CαH—$C\beta_{nonp}$, since aromatic C—H resonating at >145 ppm is impossible in arene rings, but normal for furan with a protonated α-carbon.

Both samples show characteristic arene peaks around (125 ppm, 130 ppm) in the EXPANSE spectrum. The relatively low chemical shift of 130 ppm of the nonprotonated arenes indicates substitution by COO, rather than alkyl or arene, which would give ~140-ppm chemical shifts. The expected cross peaks between COO resonating near 164 ppm and aromatic (arene and furan-Cβ) carbons between 120 and 130 ppm are clearly observed in the dipolar dephased DQ/SQ spectra. It may also be due to fused rings such as benzofuran or naphthalene, see Scheme 1. Compared to Pyr350fumS, DirfumS shows a smaller arene carbon fraction.

The alkyl CH_n carbons (ω_1 = 30–60 ppm) in the EXPANSE spectrum of the DirfumS sample show various clear cross peaks. Ketone C=O bonded to alkyl CH_n is detected at 200 ppm; this low C=O chemical shift indicates linking of the ketone to an aromatic carbon. Furan O—Cα (155 ppm) and Cβ (115–125 ppm) bonded to alkyl CH_n is also prominent, while arene (140 ppm) bonded to alkyl CH_n is not abundant enough to produce a local maximum. Finally, COO (180 ppm) bonded to alkyl CH_n is also observed. Overall, comparison of the 2D spectra in Figs. 2, 5 and 6 shows that EXPANSE and dipolar-dephased DQ/SQ spectra exhibit many cross peaks that are invisible in the unselective 2D spectra.

4. Melanoidins

Figs. 7 and 8 show the EXPANSE and dipolar-dephased DQ/SQ spectra of two different melanoidins, one made in the solid state with moderate glycine concentration (9:1 glucose:glycine), the other in solution with a 1:1 glucose:glycine molar ratio. They exhibit cross peak patterns that are dramatically different from each other and from those of the sulfuric-acid treated glucose-based materials, both for the aromatic and the alkyl regions.

The 9:1 solid-state melanoidin, Mel9:1, provides a clear example of a material with furan rings that are predominantly substituted or linked via Cα, mostly by alkyl groups: O—Cα at ~152 ppm is mostly not protonated and shows a pronounced cross peak with various alkyl carbons, see Fig. 7a. In the EXPANSE spectrum, the signal near (109 ppm, 120 ppm) from nonprotonated Cβ

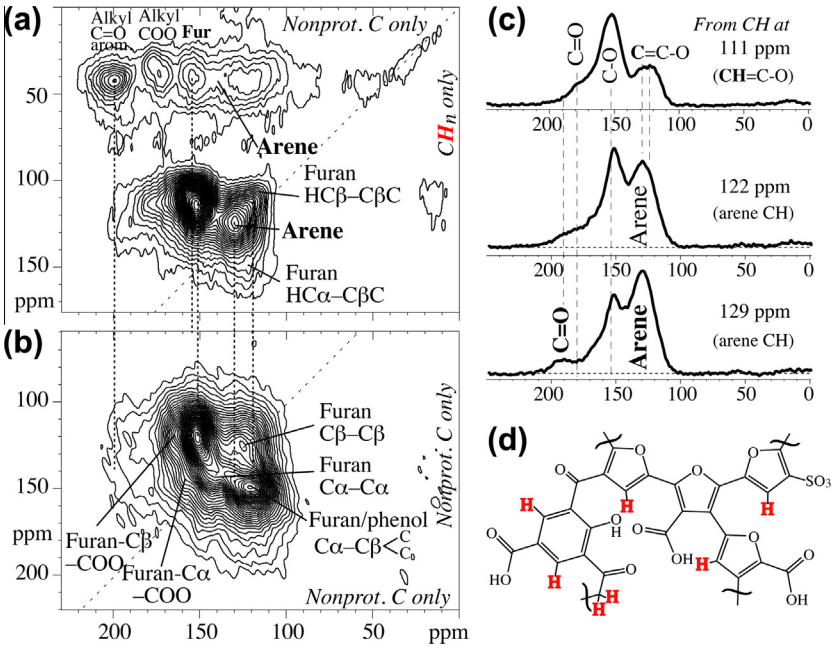

Fig. 5. (a) EXPANSE spectrum with 10-ms spin-diffusion time, and (b) sheared dipolar-dephased DQ/SQ NMR spectrum of ^{13}C-labeled glucose carbonized by treatment with fuming sulfuric acid (DirfumS). The diagonal in the spectra (at $\omega_2 = \omega_1$) is indicated by a dashed line. Many of the cross peaks clearly seen in these spectra could not be observed in the corresponding unselective 2D spectrum of Fig. 2a. (c) Horizontal cross sections from the spectrum in (a) at CH chemical shifts of 111, 122, and 129 ppm. Note that the arene peak observed in the 122- and 129-ppm cross sections is completely obscured by the furan signals in the unselective spectra of Figs. 1a and 2a. (d) Partial structural model indicating some of the furan and arene rings and their connectivities deduced from the spectra in (a) and (b).

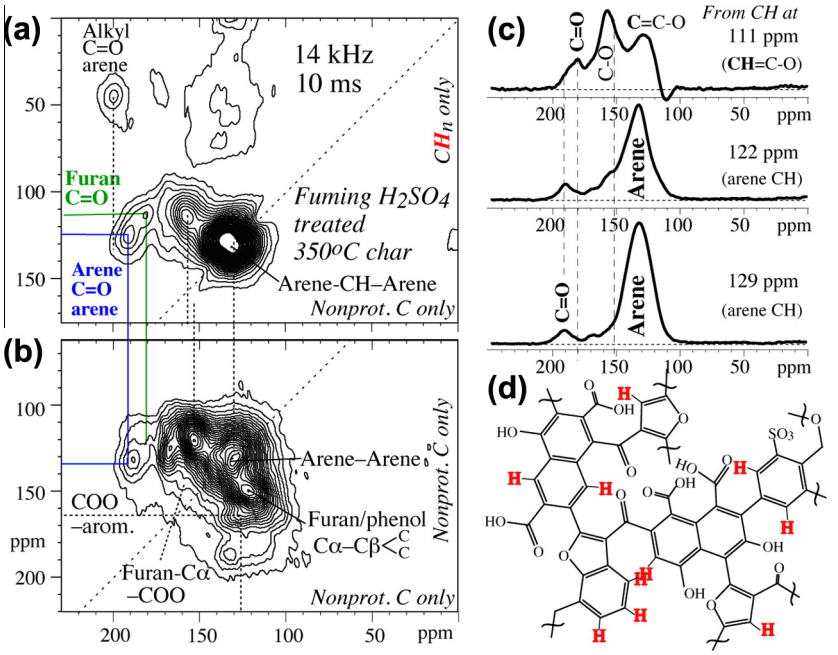

Fig. 6. (a) EXPANSE (t_m = 10 ms) and (b) sheared dipolar-dephased DQ/SQ NMR spectra of ^{13}C-labeled glucose carbonized by pyrolysis at 350 °C and treatment with fuming sulfuric acid (Pyr350fumS). In (b), note the absence of a strong peak near the diagonal at 130 ppm from pairs of nonprotonated arene carbons, which would be found in fused aromatic clusters (while the arene HC—C_{nonp} signal is prominent in a). (c) Horizontal cross sections from the spectrum in (a) at CH chemical shifts of 111, 122, and 129 ppm. (d) Partial structural model indicating some of the arene and furan rings and their connectivities deduced from the spectra in (a) and (b).

next to protonated Cβ is much weaker than in the sulfuric-acid treated carbon materials, confirming that most Cβ in this melanoidin are protonated and do not contribute much to the linkage of the furan rings.

The dipolar-dephased DQ/SQ spectrum, see Fig. 7b, is of fairly low intensity since bonded nonprotonated carbons are relatively rare in this material: Its nonprotonated furan O—Cα is mostly bonded to protonated Cβ and to protonated alkyl C, while the nonprotonated C=O is mostly bonded to protonated alkyl C, and COO is rare (see Fig. 1f). Weak signals of furan O—Cα—Cα—O and, less clearly, Cβ—Cβ linkages are observed near the diagonal at 150 and 120 ppm, respectively, and nonprotonated Cα—Cβ cross peaks are also less pronounced than for the sulfuric-acid treated carbon materials. Arene signals, which were clearly identified in the EXPANSE

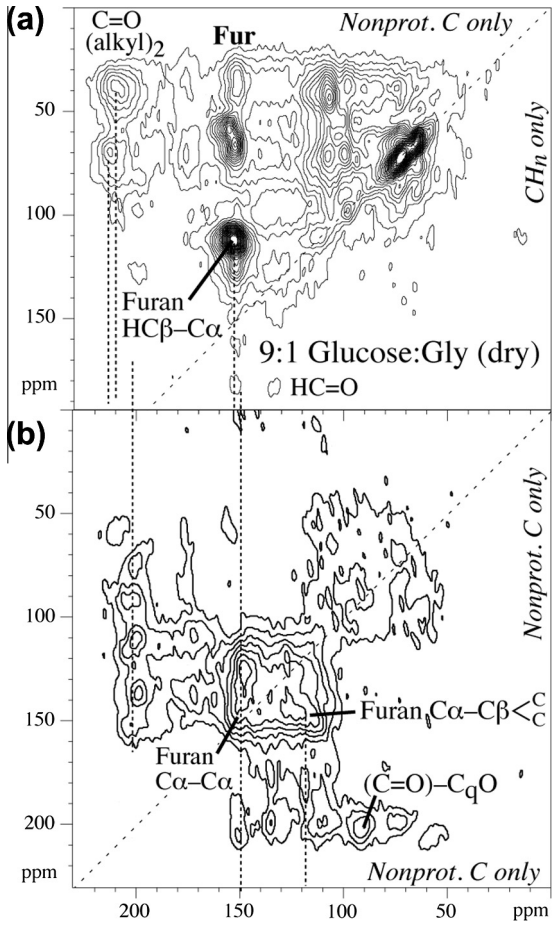

Fig. 7. (a) EXPANSE (t_m = 10 ms) and (b) sheared dipolar-dephased DQ/SQ NMR spectrum of a high-molecular weight melanoidin made from glycine and ^{13}C-enriched glucose in 9:1 M ratio at 125 °C by dry reaction of coprecipitated powder (Mel9:1). Signals characteristic of furans (alkyl C bonded to aromatic C—O, labeled "Fur") are clearly detected. The low spectral intensity in (b) can be attributed to the low abundance of directly bonded nonprotonated carbons in this material.

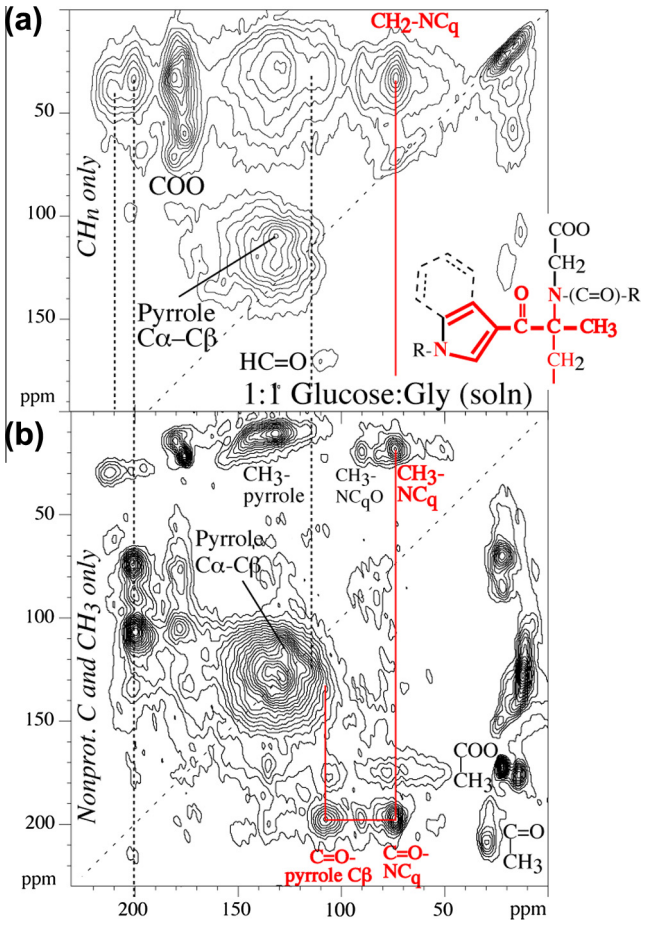

Fig. 8. (a) EXPANSE (t_m = 10 ms) and (b) sheared dipolar-dephased DQ/SQ NMR spectrum of a high-molecular weight melanoidin made from glycine and ^{13}C-enriched glucose in 1:1 M ratio in solution at 99 °C (Mel1:1). Sharp peaks from a sequence of carbons in a specific structural fragment (see proposed structure in (a) and in the Supplementary material) are connected by a continuous red line. (For interpretation of the references to color in this figure legend, the reader is referred to the web version of this article.)

spectra of the sulfuric-acid treated carbon materials, are of low intensity in this melanoidin.

Further, the series of cross peaks near 70 ppm in the EXPANSE spectrum shows that these signals are not from separate regions with incompletely pyrolyzed glucose, but are structurally integrated with the furan and C=O groups. The same can be said of the other alkyl segments, which also show a variety of cross peaks.

For the solution melanoidin, Mel1:1, the characteristic signals of Cα-substituted furan observed in the EXPANSE spectra of all the other materials are very weak. Instead, Fig. 8a shows a broad signal around (111 ppm, 135 ppm) that is indicative of Cα-substituted pyrroles. In the dipolar dephased DQ/SQ spectrum, see Fig. 8b, a pronounced signal at (120 ppm, 130 ppm) can be assigned to pyrrole Cβ—Cα—N. Given that both carbons involved must be nonprotonated, this suggests significant substitution on both Cα and Cβ. By comparison, the (120 ppm, 120 ppm) near-diagonal ridge from Cβ—Cβ linkages is less pronounced. The 2D spectra show broad peaks near 123 ppm, which may be a superposition of arene and pyrrole signals. While the signal at (125 ppm, 132 ppm) is characteristic of arene rings in N-free carbon materials, in melanoidins and other N-rich systems imidazolium carbons are found to resonate in this range [13]. This ambiguity can be eliminated using ^{13}C{^{15}N} recoupled dipolar dephasing [13], see Fig. S1b, which indicates that N-containing aromatic rings are more common than arene rings.

In the dipolar dephased DQ/SQ spectrum of this melanoidin, see Fig. 8b, the signals of various C=O/COO/NC=O carbons and CH_3 groups stand out (while the solution melanoidin showed hardly any CH_3 peaks). The former are mostly bonded to various alkyl CH_n, the latter to pyrrole Cα and Cβ, C=O (e.g. in acetyl or N-acetyl groups), and nonprotonated alkyl carbons. The CH_3 groups and some of the COO moieties are end groups, but the effect on connectivity is balanced by nonprotonated alkyl C (see dipolar dephased spectrum in Fig. 1e, and region with $\omega_2 < 110$ ppm in Fig. 8a), which are bonded to two to four C and thus act as crosslink points. A specific structural fragment identified based on three relatively sharp cross peaks is discussed below.

5. Discussion

In the following, we will discuss the signals characteristic of various aromatic rings in our new spectrally edited 2D correlation spectra. We start with a discussion of the resonance positions of ketones, which we find to be excellent indicators of their bonding partners, such as arene, furan, or alkyl groups.

5.1. Bonding of ketones and COO

The edited ^{13}C—^{13}C correlation spectra reveal a variety of signals from ketones (C=O groups), whose two bonding partners can be

identified from the cross peak frequencies. Their first bonding partner is specified directly by the alkyl or aromatic-carbon frequency of the cross peak, and the second bonding partner can be identified based on the ketone chemical shift. Chemical shift databases show that ketones can resonate over a wide frequency range, between 212 and 165 ppm, depending on the bonding partners (see Scheme S2). The data compiled in Table 1 demonstrate that the ketone chemical shift is decreased most by bonding to furan Cα, then Cβ, and much less by bonding to arenes/phenols. The same trend is observed for COO groups (see Scheme S3 and the last row of Table 1), but the total shift range is smaller since COO groups have only a single bonding partner. On the basis of Table 1, COO and C=O signals, whose chemical shift ranges overlap near 180 ppm, can be correctly assigned when a cross peak specifies one bonding partner; some examples are given in the following paragraphs.

The EXPANSE spectra of the melanoidins in Figs. 7 and 8 show signals of C=O at 210 ppm bonded to an alkyl C at 40 ppm; the high ppm value of the ketone requires another alkyl C as the second bonding partner, according to Table 1. Ketones resonating at 200 ppm and showing a cross peak to an alkyl C at 34 ppm in Fig. 8 must be bonded to an aromatic, and most likely arene, carbon (see Table 1); the corresponding cross peak at (200 ppm, 134 ppm) is indeed observed in the DQ/SQ spectrum.

The spectra of the sulfuric-acid treated materials exhibit ketone signals at <200 ppm, as expected due to their predominantly aromatic structure. A cross peak near 180 ppm to any aromatic chemical shift (between 155 and 100 ppm) must be assigned to a C=O group, since COO bonded to aromatics resonates at <169 ppm (Table 1). Pyr350fumS shows pronounced ridges ending at (125 ppm, 190 ppm) and (135 ppm, 190 ppm) in the EXPANSE and DQ/SQ spectra, respectively. Based on the 135-ppm chemical shift, which is very rare in furans, these signals must be assigned to C=O bonded to arene C. According to Table 1, the 190-ppm C=O frequency indicates that the other bonding partner must be an aromatic C, most likely a furan Cβ, which is consistent with the furan-rich sample composition. Consistently, the DQ/SQ spectrum shows intensity at (∼120 ppm, 190 ppm).

Overall, the analysis presented here demonstrates that ketones can serve as excellent indicators of their environment, and can identify arenes in particular. This can be exploited even without isotopic enrichment, since the ketone peak positions can also be determined in one-dimensional spectra of ^{13}C in natural abundance.

5.2. Signals characteristic of arenes

The EXPANSE spectra of Pyr350fumS and DirfumS, see Figs. 5a and 6a, show several signals characteristic of arenes. The most telling are (i) the cross peak between CH at ∼123 ppm and nonprotonated C at 131 ppm, and (ii) the cross peak between alkyl C (<90 ppm) and arene, specifically near 140 ppm, which is the resonance position of a nonprotonated arene carbon with a single bond to a substituent.

The C=O signals in the EXPANSE spectra also provide evidence of arenes (in the nitrogen-free materials). They show alkyl—C=O cross peaks at (40 ppm, 200 ppm). The C=O resonance frequency indicates that the other substituent of the C=O are most likely arenes, since Table 1 shows that C=O bonded to furan usually resonates at $\leqslant$195 ppm and alkyl-C=O-alkyl at $\geqslant$205 ppm. Confirming this analysis, the (40 ppm, 200 ppm) cross peak is seen particularly clearly in the sulfonated 350 °C carbon, see Fig. 6a, where arenes are known to be the major species. The spectrum of the DirfumS sample, see Fig. 5a, also exhibits this cross peak, and no peak near (40 ppm, 190 ppm), indicating that ketones link alkyl groups mostly to arenes and not furans.

Cross peaks at (125 ppm, 190 ppm) in the EXPANSE and at (135 ppm, 190 ppm) in the DQ/SQ spectrum of the nitrogen-free materials, see Figs. 5 and 6, must be assigned to C=O bonded to an arene ring, based directly on the arene chemical shift in ω_1. With ω_2 = 190 ppm, according to Table 1 the second bonding partner is arene or furan Cβ; note that the peak in EXPANSE must be from a two-bond correlation, since aromatic CH cannot be directly bonded to C=O.

The dipolar-dephased DQ/SQ spectrum can provide some information about bonds *between* aromatic rings. A bond between two arene rings will result in signal near the diagonal around 140 ppm (while a Cα—Cα linkage of furans produces near-diagonal signal around 145 ppm). Generally, if two ring carbons of the same type are linked, the signals are close to the diagonal, where they would be impossible to observe in a simple spin-exchange spectrum without spectral editing.

5.3. Signals characteristic of fused aromatic rings

The abundant interior (bridgehead) carbons of graphene-like fused aromatic rings, which are not protonated and bonded to at least one, and often to three, similar nonprotonated bridgehead carbon, would produce a characteristic strong peak near (130 ppm, 130 ppm) in the dipolar-dephased DQ/SQ spectrum. Such a signal is not observed in any of the samples studied here. However, it dominates the spectrum of glucose pyrolyzed at 450 °C (data not shown). Note that this peak on the spectral diagonal would be undetectable in a conventional 2D exchange spectrum due to both the presence of the diagonal ridge and the strong overlap with the arene CH—$C_{nonprot}$ cross peak (seen prominently near the diagonal in the EXPANSE spectrum of Pyr350fumS, see Fig. 6a).

Table 1
Chemical shifts (in ppm) of ketones R_1—(C=O)—R_2 for different substituents R_1 and R_2, as well as R_1—COOH (fixed R_2=OH), from empirical chemical-shift predictions (ACD/NMR predictors); the chemical structures used are shown in Scheme S2 in the Supplementary material. The average chemical shift change in ppm induced by each substituent (relative to ethyl) is also given. Secondary substituents (on R_1 and R_2) vary the C=O chemical shifts by approximately ±5 ppm. Entries not in bold font repeat values on the other side of the diagonal in the table.

Substituent R_1 / R_2	Ethyl	Methyl (−3)	Phenol (o-) (−3)	Arene (−9)	Pyrrole Cβ (−13)	Furan Cβ (−15)	Pyrrole Cα (−17)	Furan Cα (−20)
Ethyl	**212**	207	206	200	196	195	193	189
Methyl (−3)	**207**	**206**	203	198	193	192	189	185
Phenol (o-; −3)	**206**	**203**	**200**	201	193	195	188	186
Arene (−9)	**200**	**198**	**201**	**197**	190	188	185	182
Pyrrole Cβ (−13)	**196**	**193**	**193**	**190**	**184**	183	180	178
Furan Cβ (−15)	**195**	**192**	**195**	**188**	**183**	**176**	180	175
Pyrrole Cα (−17)	**193**	**189**	**188**	**185**	**180**	**180**	**174**	174
Furan Cα (−20)	**189**	**185**	**186**	**182**	**178**	**175**	**174**	**165**
R_2=OH (−30) (i.e., COOH)	**181**	**178** acetic acid	**171**	**168**	**166**	**165**	**163**	**163**

5.4. Signals characteristic of furans

The selective 2D correlation spectra contain several signals characteristic of furans and impossible or unlikely in phenols. The most telling signals are (i) the cross peaks between the aromatic C—O (~150 ppm) and alkyl C (<90 ppm); the corresponding linkage is impossible in a phenol, where the C—O carbon is always bonded to two aromatic C (see Scheme 1b). These furan signals can be seen very clearly in the EXPANSE spectra of DirfumS and Mel9:1, see Figs. 5a and 7a, and in the dipolar-dephased DQ/SQ spectra, see Figs. 5b and 7b, for CH_3 groups (whose signals survive the dephasing due to motional averaging of the C—H dipolar coupling) in the same samples.

A second characteristic of furans is (ii) signal from two carbons bonded to one another that are each two bonds from oxygen, i.e. both resonate between 105 and 125 ppm. These occur automatically in every furan ring, namely the two Cβ carbons, while a very special arrangement of two phenols would be required to produce this constellation. If at least one of these Cβ carbons is not bonded to H (which is commonly only in DirfumS), signals from the Cβ pairs are observed near (111 ppm, 120 ppm) in the EXPANSE spectrum (if one Cβ is protonated), or at (120 ppm, 120 ppm) in the dipolar-dephased DQ/SQ spectrum (if both are not protonated), see Fig. 5.

Thirdly, C=O and COO groups bonded to furan Cα or Cβ show large shifts by ca. −10 to −15 ppm relative to those in phenols or other arenes, see Table 1. Thus, when bonded to furans, COO groups can resonate between 160 and 165 ppm, and C=O groups between 165 and 195 ppm. Indeed, Figs. 1c and 5b show indications of COO signals below 165 ppm. The signals observed near (112 ppm, 180 ppm) in the EXPANSE spectrum, particularly clearly in Fig. 6a and c, must be attributed to C=O bonded to furan (since C=O bonded to phenols has no signals in this range, see Table 1). We can also conclude that these C=O groups cannot be bonded to an alkyl carbon, since they would then resonate between 185 and 200 ppm (see Table 1). This is indeed correct, since this sample is almost free of alkyl components.

5.5. Signals characteristic of phenols

A cross peak of the Cγ carbons in a phenol, which would usually resonate between 130 and 140 ppm, with a Cβ resonance between 105 and 125 ppm, would be characteristic of phenol. Since every phenol has two β and two γ carbons, this signal should be quite pronounced if phenols were significantly present. Our spectra do not show prominent peaks of this kind, although some may be hidden by other, stronger signals.

Bonding of functional groups to phenol Cα is not possible, and C=O or COO groups bonded to phenol Cβ resonate at relatively "normal" chemical shifts of ~200 ppm or ~168 ppm, respectively. Since the substituted phenol Cβ and the C=O(O) carbons are both not bonded to H, their signal would be observed in the dipolar-dephased DQ/SQ spectrum at (120 ppm, 200 ppm) or (120 ppm, 168 ppm). Such signals are not seen prominently in our spectra.

Another characteristic of phenols is the arene O—H proton signal near 8 ppm, which is not dephased in MELODI-filtered $^{1}H—^{13}C$ correlation experiments [40] (not shown here). None of the samples studied here showed a pronounced phenol OH signal.

5.6. Identification of differently linked furans

The EXPANSE and dipolar-dephased DQ/SQ spectra can identify whether the furans are predominantly substituted on Cα, Cβ, or both, since they probe the protonation of these carbons. For instance, the signals at $\omega_1 = 111$ ppm in the EXPANSE spectra of DirfumS and Mel9:1, see Figs. 5a and 7a, can both be attributed to Cβ—H in furan, but the different cross peak intensity near 120 ppm indicates a structural difference.

According to our experimental design, this 120-ppm band, which is strong for the DirfumS material, see Fig. 5c, must be due to a nonprotonated carbon. This rules out arene CH and leaves only nonprotonated aromatic C separated from oxygen or nitrogen by two bonds. Such a carbon will be found naturally as the second β-carbon in a furan ring next to the Cβ—H resonating near 111 ppm, which was selected in the ω_1 dimension by our experimental design, see Fig. 4. This second β-carbon, being nonprotonated, must be bonded to another carbon outside the furan ring. In the spectrum of the Mel9:1 sample, see Fig. 7a, the 120-ppm signal is not pronounced, which tells us that the β-carbons in these furan rings are mostly protonated and therefore do not show up in the ω_2 dimension of our EXPANSE spectrum. This matches the absence of a strong peak of nonprotonated Cβ—Cα—O pairs in the dipolar dephased DQ/SQ spectrum, as well as our previous observations [14] and the accepted picture that the furan rings in melanoidins are linked to other units mostly via their α-carbons. By contrast, spectral features such as the strong nonprotonated Cβ—Cα—O cross peak in Fig. 5b show that many of the β-carbons in the furan rings of sulfuric-acid treated glucose (DirfumS) are not bonded to H.

When Cα is bonded to H but Cβ is not, a cross peak will be observed at (145 ppm, 120 ppm) in the EXPANSE spectrum. A broad signal of this kind is indeed observed for the DirfumS sample, see Fig. 5a. An intermolecular Cβ—Cβ linkage will always give a signal near the diagonal around 120 ppm in the dipolar dephased DQ/SQ spectrum; intramolecular Cβ—Cβ cross peaks have been discussed above.

5.7. Nonprotonated O—Cα—Cβ

Peaks of nonprotonated O—Cα—Cβ pairs at (150 ppm, 120 ppm) dominate the dipolar-dephased DQ/SQ spectra of the sulfuric-acid treated carbon materials, see Figs. 5b and 6b. Without the spectral editing, these signals would be trivial, since O—Cα is always bonded to Cβ, while the information that both carbons are not protonated reveals a valuable structural insight. In the spectra of the melanoidins, see Figs. 7b and 8b, this signal is weak, confirming [14] that furan with nonprotonated Cβ is rare in these materials.

5.8. Structure of sulfuric-acid carbonized glucose and 350 °C carbon

The cross peaks discussed provide fairly comprehensive structural pictures of DirfumS and Pyr350fumS; resulting simple structural models are shown in Figs. 5d and 6d, respectively. The DirfumS material consists mostly of a network of furan rings heavily substituted on both Cα and Cβ, by other furan rings or by COO and C=O groups. Alkyl segments and arene rings have also been detected unambiguously, but represent only relatively minor components in this material. The Pyr350fumS material consists of single and double aromatic rings, mostly arene, but also some furan, again with direct and C=O linkages as well as COO substitution. Large clusters of fused aromatic rings are rare.

5.9. Characteristic structural fragment in solution melanoidin

In our previous studies [13,14], the structure of the melanoidin from solution reaction appeared to be particularly complex and unsuitable for a detailed analysis. However, the dipolar dephased DQ/SQ spectrum in Fig. 8b shows a series of relatively sharp peaks (connected by red lines) that reveal a distinct structural fragment accounting for most of the ketones and a significant fraction of all carbons in this material. We start the analysis with the two peaks at 72 ppm. They are due to a nonprotonated alkyl carbon that is bonded to CH_3 (top cross peak at 15 ppm) and to C=O

(bottom cross peak at 200 ppm). The remaining carbon substituent of the 72-ppm C is protonated and therefore observed in the EXPANSE spectrum in Fig. 8a, where it is seen to resonate at 32 ppm, which is quite characteristic of methylene groups [14]. The nonprotonated alkyl carbon is bonded to nitrogen (i.e. it is NC_q) as proved by $^{13}C\{^{15}N\}$ dipolar dephasing (see Fig. S1b) and consistent with the chemical shift (while OC_q would resonate at >80 ppm; such a signal is also observed, at lower intensity). Thus, we have identified all four bonding partners of the NC_q carbon:CH_3, C═O, CH_2, and N.

While the CH_3 groups cannot have a second carbon bonded, the 200-ppm C═O group must have one. That carbon resonates at 107 ppm, as evidenced by a sharp cross peak in Fig. 8b. We assign it to the β-carbon of a pyrrole or related heterocycle (most likely indole) based on several arguments: Spectral editing showed little nonprotonated alkyl carbon signal at 107 ppm (see Fig. S1d); in addition, the chemical shift of a ketone bonded to two alkyl carbons would be >205 ppm, not the observed 200 ppm (see Table 1). Furans, whose β-carbons could also resonate around 115 ppm, are not common in this material, as evidenced by the absence of their characteristic cross peaks at 150 and ~115 ppm in the spectra of Fig. 8. The low (107 ppm) chemical shift value suggests possibly a second heteroatom in the aromatic ring, or a fused arene ring forming an indole structure, which consistently results in a very low chemical shift of the β-carbon of interest here [25], similarly as for the corresponding carbon in benzofuran, see Scheme 1c. Overall, the seven carbons (CH_3, CH_2, NC_q, C═O, and three pyrrolic) clearly identified account for ca. 15% of the total in this melanoidin.

A similar set of cross peaks was observed in a solution glucose–glycine melanoidin (termed nitrogen-containing hydrothermal carbon) prepared at 180 °C for 12 h by Baccile et al. [15]. For ease of comparison with the (unselective) DQ/SQ spectrum in Fig. 5 of Ref. [15], Fig. S1e shows the dipolar dephased DQ/SQ spectrum of our sample in the format of Ref. [15], without shearing. However, the corresponding peaks in Ref. [15] were assigned to a quite different, O—CH_2—(C═O)—C(OH,R′)—COO, structure, with "R′═H, OH" (see Fig. S1a). Thus, the 72-ppm signal was assigned to O—CH_2, not NC_q, and the 107-ppm signal to alkyl $C(OH)_2$, not to aromatic Cβ of pyrrole.

Our spectral editing conclusively shows that O—CH_2—(C═O)—C(OH,R')—COO is not the structural fragment in our sample, and the spectral evidence in Ref. [15] supports this conclusion for their sample also. The lack of dipolar dephasing in our spectra shows that the signal at 72 ppm is not from an OCH_2 group, but from a nonprotonated carbon; the absence of this signal from the short-CP spectrum shown in Ref. [15] indicates that this is also true for the sample in Ref. [15]: CH_2 signal would be strong under those conditions, while nonprotonated C is not. $^{13}C\{^{15}N\}$ REDOR [14] further shows that this nonprotonated carbon is bonded to N (see Fig. S1b), which also explains its chemical shift.

The proposed identification of the other bonding partner of the C═O group is also doubtful based on further spectral editing. In Ref. [15], its 107-ppm signal was assigned to an sp^3-hybridized $C(OH)_2$ carbon, but chemical-shift anisotropy filtering [41] of both 1D and DQ/SQ spectra, see Figs. S1c–S1f, suppresses this signal, which means that it must be sp^2-hybridized.

This example highlights that cross peak positions alone are not sufficient for correct structural analysis of complex organic materials, and spectral editing is needed for correct structure determination.

6. Conclusions

We have presented two complementary methods for obtaining spectrally edited 2D ^{13}C—^{13}C spectra of ^{13}C-enriched carbon materials. Both require only moderate radio-frequency power and give spectra free of a diagonal ridge and the spectral artifacts associated with it. The spectra specifically provide correlations between two nonprotonated carbons, or one nonprotonated C and one CH_n, which combined with the two chemical-shift coordinates of the cross peak define the local bonding environment. We have pointed out cross peaks, including several near the diagonal and others involving ketones, that are characteristic of arenes, clusters of fused aromatic rings, or furans. Different substitutions or linkages of furan rings can also be distinguished. Our revision of a published structure proposed for a solution melanoidin based on unselective DQ/SQ NMR demonstrates the importance of spectral editing for correct structure determination.

7. Experimental section

7.1. Materials

Uniformly ^{13}C-enriched glucose and ^{15}N-enriched glycine were purchased from Cambridge Isotopes.

7.1.1. Pyrolyzed carbon preparation

One to two grams of uniformly ^{13}C-enriched glucose was loaded into a horizontal tube furnace purged with nitrogen gas (99.995% purity, purchased from Airgas) flowing at about 1 L/min for 1 h prior to heating, and heated to 350 °C with a rate of 10 °C/min and held at the temperature for 1 h. To ensure uniform heat transfer and homogeneity, the materials were cooled and ground into a fine powder with a mortar and pestle. This material was then subjected to additional reaction for 9 h using the same nitrogen flow rate and heating program.

7.1.2. Sulfonation of glucose and carbon materials by fuming sulfuric acid

Glucose dehydrates in concentrated sulfuric acid to a char similar in appearance to pyrolytic carbons. In previous literature, this direct dehydration provided high sulfur incorporation [4].

Fuming sulfuric acid was prepared by addition of sulfur trioxide to neat sulfuric acid, immediately prior to the sulfonation reactions. Sulfonation was carried out by addition of either uniformly ^{13}C-enriched glucose ("DirfumS") or the ^{13}C-enriched 350 °C carbon ("Pyr350fumS") into an Erlenmeyer flask with about 150 mL of 30% fuming sulfuric acid and heated to 150 °C for 2 h. The resulting black solid was then washed and filtered (4.5–5 μm Buchner funnel) with ~2–3 L of DI water until the solution was clear, colorless, and of neutral pH, and no sulfate ions were detected with barium chloride. The final material was dried overnight in an oven at 100 °C. The C:H:O:S elemental compositions of the DirfumS and Pyr350fumS materials were 54:3:39:3.5 and 61:3:32:3, respectively.

7.1.3. Melanoidin synthesis

The melanoidins were synthesized using standard procedures as described in Ref. [13]. The first melanoidin was obtained by heating uniformly ^{13}C-enriched D-glucose and ^{15}N-labeled glycine in equimolar ratio in a sealed pH 8.5 buffer solution at 100 °C for a week. The pH was maintained at 8.5 and the reaction continued for an additional 5 days. This solution-phase melanoidin is termed Mel1:1. A dry-reaction melanoidin (Mel9:1) was synthesized by dissolving glucose and glycine in 9:1 molar ratio in water and co-precipitation by freeze-drying. The precipitate was then heated in an oven at 125 °C for 2 h. Both materials were filtered, dialyzed and freeze-dried prior to the NMR experiments.

7.2. NMR parameters

The NMR experiments were performed on a Bruker Avance 400 spectrometer at a 100 MHz ^{13}C resonance frequency, using a 4-mm double-resonance probehead. All the 2D spectra were measured at a spinning frequency of $\nu_r = 14$ kHz, where spinning sidebands are fairly small and have little overlap with centerbands. ^{13}C and ^{1}H 90° pulse lengths were 4.2 μs, and the ^{1}H decoupling field strength was $\gamma B_1/(2\pi) = 70$ kHz. The recycle delay in most experiments presented was 0.8–1 s. One-dimensional 1-ms cross-polarization spectra were recorded at 7.8 kHz and 4 kHz with total suppression of spinning sidebands (TOSS) [36]. The mixing time in the EXPANSE experiments was 10 ms, while the DQ excitation and reconversion in the DQ/SQ experiments consisted of two periods of SPC5 homonuclear recoupling of 4 $t_r = 286$ μs duration each. The evolution time was incremented by $t_r/2 = 35.71$ μs in EXPANSE and $t_r/4 = 14.28$ μs in DQ/SQ experiments, and reached a maximum of 0.9 ms and 1 ms, respectively. Other parameters of the new 2D experiments are given under Section 2.

7.3. Chemical-shift calculations

The chemical shifts shown in Scheme 1 and Table 1 were calculated using the commercially available, empirically based ACD chemical-shift predictors. The complete molecules used to generate the chemical shifts given in Scheme 1 are shown in Scheme S1 in the Supplementary material, and represent structures that are likely to be found in the materials studied given the functional groups and their connectivities determined in the 2D NMR spectra. Table 1 was produced by systematically varying the substituents bonded to ketones, including methyl, ethyl, arene, phenol, pyrrole Cα/Cβ, and furan Cα/Cβ. The complete set of simulated structures is shown in Scheme S2. The chemical shifts for the carboxylic acids were simulated for structures, shown in Scheme S3, that are found in our structural models of the sulfonated carbon materials. Additionally, experimental chemical shift values were looked up in the SDBS database for organic compounds [42], and were found to be in good agreement with the trends from the ACD chemical shift simulator.

Acknowledgment

This work was supported by the Center for Biorenewable Chemicals (CBiRC) funded by NSF Grant EEC-0813570.

Appendix A. Supplementary material

Supplementary data associated with this article can be found, in the online version, at http://dx.doi.org/10.1016/j.jmr.2013.06.006.

References

[1] M.-M. Titirici, M. Antonietti, N. Baccile, Hydrothermal carbon from biomass: a comparison of the local structure from poly- to monosaccharides and pentoses/hexoses, Green Chem. 10 (2008) 1204–1212.
[2] M. Antonietti, K. Müllen, Carbon: the sixth element, Adv. Mater. 22 (2010) 787.
[3] B. Hu, K. Wang, L. Wu, S.-H. Yu, M. Antonietti, M.-M. Titirici, Engineering carbon materials from the hydrothermal carbonization process of biomass, Adv. Mater. 22 (2010) 813–828.
[4] V. Mirkhani, M. Moghadam, S. Tangestaninejad, I. Mohammadpoor-Baltork, M. Mahdavi, Preparation of an improved sulfonated carbon-based solid acid as a novel, efficient, and reusable catalyst for chemoselective synthesis of 2-oxazolines and bis-oxazolines, Monatsh. Chem. 140 (2009) 1489–1494.
[5] L. Zhao, L.-Z. Fan, M.-Q. Zhou, H. Guan, S. Qiao, M. Antonietti, M.-M. Titirici, Nitrogen-containing hydrothermal carbons with superior performance in supercapacitors, Adv. Mater. 22 (2010) 5202–5206.
[6] M.-M. Titirici, M. Antonietti, Chemistry and materials options of sustainable carbon materials made by hydrothermal carbonization, Chem. Soc. Rev. 39 (2010) 103–116.
[7] D.A. Laird, The charcoal vision: a win–win–win scenario for simultaneously producing bioenergy, permanently sequestering carbon, while improving soil and water quality, Agronomy J. 100 (2008) 178–181.
[8] C.E. Brewer, K. Schmidt-Rohr, J.A. Satrio, R.C. Brown, Characterization of biochar from fast pyrolysis and gasification systems, Environ. Progr. Sustain. Energy 28 (2009) 386–396.
[9] J.-D. Mao, R.L. Johnson, J. Lehmann, D.C. Olk, E.G. Neves, M.L. Thompson, K. Schmidt-Rohr, Abundant and stable char residues in soils: implications for soil fertility and carbon sequestration, Environ. Sci. Technol. 46 (2012) 9571–9576.
[10] C.M. Preston, M.W.I. Schmidt, Black (pyrogenic) carbon: a synthesis of current knowledge and uncertainties with special consideration of boreal regions, Biogeosciences 3 (2006) 397–420.
[11] K. Hammes, M.W.I. Schmidt, R. Smernik, L.A. Currie, W.P. Ball, T.H. Nguyen, P. Louchouran, S. Houel, O. Gustafsson, M. Elmquist, G. Cornellisen, J.O. Skjemstad, C.A. Masiello, J. Song, P.a. Peng, S. Mitra, J.C. Dunn, P.G. Hatcher, W.C. Hockaday, D.M. Smith, C. Hartkopf-Froder, A. Bohmer, B. Luer, B.J. Huebert, W. Amelung, S. Brodowski, L. Huang, W. Zhang, P.M. Gschwend, D.X. Flores-Cervantes, C. Largeau, J.-N. Rouzand, C. Rumpel, G. Guggenberger, K. Kaiser, A. Rodionov, F.J. Gonzalez-Perez, J.A. Gonzalez-Perez, J.M. De la Rosa, D.A.C. Manning, E. Lopez-Capel, L. Ding, Comparison of quantification methods to measure fire-derived (black/elemental) carbon in soils and sediments using reference materials from soil, water, sediment and the atmosphere, Global Biogeochem. Cycles 21 (2007) 6.
[12] A. Golon, N. Kuhnert, Unraveling the chemical composition of caramel, J. Agric. Food Chem. 60 (2012) 3266–3274.
[13] X.-W. Fang, K. Schmidt-Rohr, The Fate of the amino acid in glucose–glycine melanoidins investigated by solid-state NMR, J. Agric. Food Chem. 57 (2009) 10701–10711.
[14] X. Fang, K. Schmidt-Rohr, Alkyl and other major structures in ^{13}C-labeled glucose–glycine melanoidins identified by solid-state nuclear magnetic resonance, J. Agric. Food Chem. 59 (2010) 481–490.
[15] N. Baccile, G. Laurent, C. Coelho, F. Babonneau, L. Zhao, M.-M. Titirici, Structural insights on nitrogen-containing hydrothermal carbon using solid-state magic angle spinning ^{13}C and ^{15}N nuclear magnetic resonance, J. Phys. Chem. C 115 (2011) 8976–8982.
[16] W. Cai, R.D. Piner, F.J. Stadermann, S. Park, M.A. Shaibat, Y. Ishii, D. Yang, A. Velamakanni, S.J. An, M. Stoller, J. An, D. Chen, R.S. Ruoff, Synthesis and solid-state NMR structural characterization of ^{13}C-labeled graphite oxide, Science 321 (2008) 1815–1817.
[17] W. Gao, L.B. Alemany, L. Ci, P.M. Ajayan, New insights into the structure and reduction of graphite oxide, Nat. Chem. 1 (2009) 403–408.
[18] M.W.I. Schmidt, J.O. Skjemstad, E. Gehrt, I. Kögel-Knabner, Charred organic carbon in German chernozemic soils, Eur. J. Soil Sci. 50 (1999) 351–365.
[19] J.A. Baldock, R.J. Smernik, Chemical composition and bioavailability of thermally altered *Pinus resinosa* (Red pine) wood, Org. Geochem. 33 (2002) 1093–1109.
[20] M.S. Solum, J.M. Veranth, Y.-J. Jiang, A.M. Orendt, A.F. Sarofim, R.J. Pugmire, The study of anthracene aerosols by solid-state NMR and ESR, Energy Fuels 17 (2003) 738–743.
[21] J.-D. Mao, K. Schmidt-Rohr, Accurate quantification of aromaticity and nonprotonated aromatic carbon fraction in natural organic matter by ^{13}C solid state NMR, Environ. Sci. Technol. 38 (2004) 2680–2684.
[22] S.R. Kelemen, M. Afeworki, M.L. Gorbaty, M. Sansone, P.J. Kwiatek, C.C. Walters, H. Freund, M. Siskin, A.E. Bence, D.J. Curry, M. Solum, R.J. Pugmire, M. Vandenbroucke, M. Leblond, F. Behar, Direct characterization of kerogen by X-ray and solid-state ^{13}C nuclear magnetic resonance methods, Energy Fuels 21 (2007) 1548–1561.
[23] K. Hammes, R.J. Smernik, J.O. Skjemstad, M.W.I. Schmidt, Characterisation and evaluation of reference materials for black carbon analysis using elemental composition, colour, BET surface area and ^{13}C NMR spectroscopy, Appl. Geochem. 23 (2008) 2113–2122.
[24] N. Baccile, G. Laurent, F. Babonneau, F. Fayon, M.-M. Titirici, M. Antonietti, Structural characterization of hydrothermal carbon spheres by advanced solid-state MAS ^{13}C NMR investigations, J. Phys. Chem. C 113 (2009) 9644–9654.
[25] H.J. Reich, C-13 NMR Chemical Shifts (Wisconsin Data Base), 2013, <http://www.chem.wisc.edu/areas/reich/Handouts/nmr-c13/cdata.htm>.
[26] A. Bax, R. Freeman, S.P. Kempsell, Natural-abundance $^{13}C—^{13}C$ coupling observed via double-quantum coherence, J. Am. Chem. Soc. 102 (1980) 4849–4851.
[27] M. Hohwy, C.M. Rienstra, C.P. Jaroniec, R.G. Griffin, Fivefold symmetric homonuclear dipolar recoupling in rotating solids: application to double quantum spectroscopy, J. Chem. Phys. 110 (1999) 7983–7992.
[28] J. Shu, P. Li, Q. Chen, S. Zhang, Quantitative measurement of polymer compositions by NMR spectroscopy: targeting polymers with marked difference in phase mobility, Macromolecules 43 (2010) 8993–8996.
[29] G. Hou, F. Deng, S. Ding, R. Fu, J. Yang, C. Ye, Quantitative cross-polarization NMR spectroscopy in uniformly ^{13}C-labeled solids, Chem. Phys. Lett. 421 (2006) 356–360.
[30] E. Katoh, K. Takegoshi, T. Terao, ^{13}C nuclear overhauser polarization-magic-angle spinning nuclear magnetic resonance spectroscopy in uniformly ^{13}C-Labeled solid proteins, JACS 126 (2004) 3653–3657.
[31] C.R. Morcombe, V. Gaponenko, R.A. Byrd, K.W. Zilm, Diluting abundant spins by isotope edited radio frequency field assisted diffusion, JACS 126 (2004) 7196–7197.

[32] K. Schmidt-Rohr, Complete dipolar decoupling of ^{13}C, and its use in double-quantum solid-state NMR for determining polymer conformations, J. Magn. Reson. 131 (1998) 209–217.
[33] E.R. deAzevedo, W.-G. Hu, T.J. Bonagamba, K. Schmidt-Rohr, Principles of centerband-only detection of exchange in solid state NMR, and extentions to four-time CODEX, J. Chem. Phys. 112 (2000) 8988–9001.
[34] K. Takegoshi, S. Nakamura, T. Terao, C13—H1 dipolar-assisted rotational resonance in magic-angle spinning NMR, Chem. Phys. Lett. 344 (2001) 631–637.
[35] B.H. Meier, Polarization transfer and spin diffusion in solid-state NMR, Adv. Magn. Opt. Reson. 18 (1994) 1–116.
[36] W.T. Dixon, Spinning-sideband-free and spinning-sideband-only NMR spectra of spinning samples, J. Chem. Phys. 77 (1982) 1800–1809.
[37] H. Geen, G. Bodenhausen, Pure absorption-mode chemical exchange NMR spectroscopy with suppression of spinning sidebands in a slowly rotating solid, J. Chem. Phys. 97 (1992) 2928–2937.
[38] S.T. Burns, X. Wu, K.W. Zilm, Improvement of Spectral editing in solids: a sequence for obtaining $^{13}CH + {}^{13}CH2$-only ^{13}C spectra, J. Magn. Reson. 143 (2000) 352–359.
[39] J.-D. Mao, L. Tremblay, J.-P. Gagné, S. Kohl, J. Rice, K. Schmidt-Rohr, Natural organic matter in the Saguenay Fjord and the St. Lawrence Estuary investigated by advanced solid-state NMR, Geochim. Cosmochim. Acta 71 (2007) 5483–5499.
[40] X.L. Yao, K. Schmidt-Rohr, M. Hong, Medium- and long-distance $^{1}H—^{13}C$ heteronuclear correlation NMR in solids, J. Magn. Reson. 149 (2001) 139–143.
[41] J.-D. Mao, K. Schmidt-Rohr, Separation of aromatic-carbon ^{13}C NMR signals from di-oxygenated alkyl bands by a chemical-shift-anisotropy filter, Solid State NMR 26 (2004) 36–45.
[42] SDBS, NMR Database, <http://sdbs.riodb.aist.go.jp> (accessed November 2012).